

## LETTER

# Realizing high efficiency 532 nm laser by optimizing the mode- and impedance-matching

To cite this article: Wenxiu Yao *et al* 2021 *Laser Phys. Lett.* **18** 015001

View the [article online](#) for updates and enhancements.

## You may also like

- [Numerical Simulation of Conversion Efficiency and Beam Quality Factor in Second Harmonic Generation with Diffraction and Pump Depletion](#)  
Tadashi Kasamatsu, Hiroyuki Kubomura and Hirofumi Kan
- [A mixture of vortex terahertz radiation generation in inhomogeneous plasma by considering pump depletion](#)  
Mohammad Vaziri and A R Bahrapour
- [Optical manipulation and conversion in whispering gallery mode resonators with pump depletion](#)  
Liu Guo and Cong-Hua Yan

## Letter

# Realizing high efficiency 532 nm laser by optimizing the mode- and impedance-matching

Wenxiu Yao<sup>1</sup>, Qingwei Wang<sup>1</sup>, Long Tian<sup>1,2</sup>, Ruixin Li<sup>1</sup>, Shaoping Shi<sup>1</sup>, Jinrong Wang<sup>1</sup>, Yajun Wang<sup>1,2</sup> and Yaohui Zheng<sup>1,2</sup>

<sup>1</sup> State Key Laboratory of Quantum Optics and Quantum Optics Devices, Institute of Opto-Electronics, Shanxi University, Taiyuan 030006, People's Republic of China

<sup>2</sup> Collaborative Innovation Center of Extreme Optics, Shanxi University, Taiyuan, Shanxi 030006, People's Republic of China

E-mail: [yhzheng@sxu.edu.cn](mailto:yhzheng@sxu.edu.cn)

Received 18 August 2020

Accepted for publication 6 December 2020

Published 21 December 2020



CrossMark

## Abstract

Increasing the conversion efficiency of second harmonic generation (SHG) is an area of interest in research. We report a high-efficiency 532 nm laser generation, with a conversion efficiency of  $94.04 \pm 0.115\%$  from the pump depletion of  $98.1\% \pm 0.1\%$ , by accurately quantifying the round-trip loss and the transmissivity of the input mirror using our proposed scheme. The optimal conversion efficiency of the cavity-enhanced frequency doubling process is independent of the waist and is determined by the pump depletion, round-trip loss, and transmissivity of the input mirror. These results show that the cavity-enhanced frequency doubling process is not necessary to set the focusing parameter at the optimal single-pass conversion. These results provide a guide for future research on high-efficiency SHG.

Keywords: second harmonic generation, pump depletion, impedance-matching

(Some figures may appear in colour only in the online journal)

## 1. Introduction

Second harmonic generation (SHG), which can effectively extend a laser wavelength range by half the initial wavelength, is widely applied in the fields of nonclassical light generation [1, 2], laser microscopy imaging [3, 4], and cold atomic physics [5, 6]. In principle, a beam of arbitrary power can be upconverted to a shorter wavelength with an efficiency of 100%, in a phase-matching nonlinear crystal. In practice, the efficiency cannot reach the theoretical value because it is limited by experimental conditions, including the finite nonlinear coefficient and power density. However, the ideal value can be pursued by optimizing the experimental parameters.

SHG was first demonstrated in crystalline quartz in 1962 and it has since been a subject of intense theoretical

and experimental study [7], which aimed to obtain perfect frequency-doubling efficiency. For single-pass frequency doubling, the efficiency that fully obeys the Boyd–Kleinman (B-K) model is linearly dependent linearly on the pump intensity and quadratically dependent on the crystal length and the effective nonlinear coefficient [8]. A pump depletion of 99% (which, in lossless systems, is equivalent to the conversion efficiency) was obtained for a 50 ns pulse via a single-pass lithium niobate waveguide [9]. The pulse pump increases the peak pump intensity and the waveguide ensures a uniform transverse size in the whole interaction length, owing to its two-dimensional spatial confinement [10–13]. For the SHG of continuous-wave light, via the bulk crystal, cavity enhancement of the frequency-doubling process becomes a general technique, which is equivalent to increasing the crystal

length or pump intensity [14–22]. To completely characterize the external cavity SHG, we must additionally consider the cavity influence on the basis of the B-K model. The mode- and impedance-matching efficiencies are two important indicators when evaluating the pump coupling efficiency, which sets the upper limits of the conversion efficiency. Thermal lensing, induced by increasing the input power, changes the initial mode-matching efficiency; therefore, reducing the thermal effect is crucial for avoiding drastic changes in the mode-matching efficiency. Some general approaches were employed by using a looser focusing [23, 24], a ring frequency-doubling cavity [25–31], and an optimized crystal position [32]. The optimal impedance-matching efficiency can be obtained by optimizing the input power. The deviation of the focusing parameter from the optimal value can be compensated by increasing the input power. Owing to the low absorption of periodically poled KTiOPO<sub>4</sub> (PPKTP) at 1550 nm and 775 nm, the highest efficiency reported thus far is 95%, from the depletion measurement of an input power [33]. If absorption and scattering losses cannot be neglected, we cannot associate the pump depletion with conversion efficiency. The pump power is depleted, not only by the frequency conversion, but also by round-trip loss. Limited by losses, the conversion efficiency at 1342 nm is 93.8%, which is inferred from the pump depletion of 97.4%; the difference is dependent on the ratio between the nonlinear and linear depletion [34]. Thus, it is the premise of inferring the conversion efficiency from the pump depletion to accurately obtain the cavity parameters, including the round-trip loss  $L$ , the effective nonlinear coefficient  $d_{\text{eff}}$  and the transmissivity of the input mirror  $T$ .

Here, we report on high-efficiency SHG at 1064 nm, with a pump depletion of  $98.1 \pm 0.1\%$ . In virtue of our proposed scheme, we obtain the fitting results of the external cavity parameters ( $d_{\text{eff}}$ ,  $L$ , and  $T$ ) with small uncertainty. On this basis, the conversion efficiency is inferred to be  $94.04 \pm 0.115\%$ , which is in good agreement with the measurement result from a power meter, but with a smaller error. Moreover, the highest conversion efficiency is practically constant, at seven waist radii  $\omega_0$ , covering the range from 15 to 60  $\mu\text{m}$ , which experimentally confirms that the highest efficiency is insensitive to the waist radius  $\omega_0$ , but depends on  $L$ ,  $T$ , and the pump depletion  $\eta_{\text{pd}}$ . The results provide an important reference to achieve high-efficiency SHG.

## 2. Experimental setup

The schematic of our experimental setup for SHG is shown in figure 1. A continuous-wave single-frequency laser, made in-house, with a wavelength of 1064 nm and a maximum output power of 16 W, is used as the pump laser source. The Gaussian beam from the laser is injected into an optical isolator (OI1) to avoid the feedback beam. A wedged electro-optic modulator (EOM) [35], carried by a 56 MHz radio frequency function, is used to generate the error signals for the Pound–Drever–Hall (PDH) technique [36]. A mode cleaner (MC) is placed in front of the SHG to improve the spatial mode of the laser beam injected into the SHG, which ensures perfect mode-matching

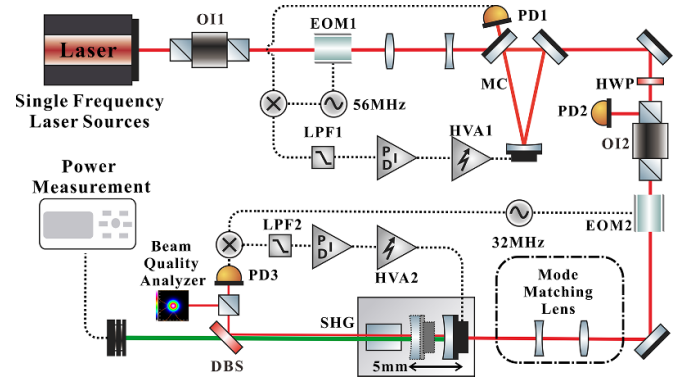


**Figure 1.** Schematic of the experimental setup. OI, optical isolator; EOM, electro-optic modulator; PD, photodetector; HWP, half-wave-plate; LPF, low-pass filter; PID, proportional-integral-derivative; HVA, high-voltage amplifier; DBS, dichroic beam splitter; MC, mode cleaner; SHG, second harmonic generation.

efficiency between the pump beam and external SHG cavity ( $98.5 \pm 0.1\%$ ). The MC resonates with the TEM<sub>00</sub> mode by the PDH scheme. The signal (PD1) extracted from the reflected light of the MC is mixed with an electronic local oscillator, the output of which is filtered by a low-pass filter and a proportional-integral-derivative controller; the acquired error signal with a high signal-to-noise ratio serves as the MC locking. The output beam of the MC is coupled into the SHG cavity after passing through another optical isolator (OI2). OI2 not only prevents the beam from returning to the MC but also monitors the reflection beam of the SHG cavity with PD2 to measure the pump power depletion. A half-wave-plate is placed in front of OI2 to adjust the pump power injecting into the SHG cavity.

In the experiment, the standing-wave SHG cavity consists of two components: one is the concave mirror, with a transmissivity of 9% at 1064 nm and a radius of curvature of 30 mm, which is attached to a piezoelectric transducer to scan or stabilize the resonator length. The other is a PPKTP crystal ( $1 \times 2 \times 10 \text{ mm}^3$ ); the poling period of the crystal is 9  $\mu\text{m}$  and the temperature is controlled by a thermoelectric peltier element and a temperature controller with a measurement precision of 0.001  $^\circ\text{C}$ . The end surface of PPKTP (Raicol Crystals Ltd) has a reflectivity of 99.95% for the fundamental wave (FW, 1064 nm) and a transmissivity of 95% for the harmonic wave (HW, 532 nm). The high reflectivity coating is designed to preserve the phase relationship between FW and HW so that it produces constructive interference of two propagating HWs [37]. Another end facet of PPKTP has the residual reflectivity of less than 0.1% at 1064 nm and 532 nm. A concave mirror is placed on a translation stage to conveniently adjust the length of the air gap between the concave mirror and the PPKTP crystal, from 20 to 24.5 mm, corresponding to the waist variation, from 15.4 to 60.3  $\mu\text{m}$ . It is worthy of noting that the waist position of the cavity in this case still locates at the outer end facet of the crystal, independent of the cavity length. The HW and FW fields are separated by a dichroic beam splitter (DBS) at the output of the SHG. The FW that is

reflected by the DBS is divided into two parts. A portion of the FW is detected by a resonant detector [38], PD3, which serves as the error signal generation of the SHG cavity locking. The other FW is injected into a beam quality analyzer (Thorlabs, BP209-VIS/M) to measure the beam parameters outside the SHG cavity. According to the propagation and transformation of Gaussian beam, the beam size inside the SHG cavity can be inferred. The HW is simultaneously detected by a power meter at the transmission end of the DBS to validate the conversion efficiency measurement.

### 3. Theoretical analysis

A standing wave frequency doubling cavity, which is quasi-phase-matched for both the forward and backward propagating intracavity beam, yields the forward and backward propagation HWs. The overall output from the constructive interference of two propagation HWs is given by [39]:

$$P_2 = 2 \times E_{nl} \times P_C^2, \quad (1)$$

where  $P_C$  is the circulating fundamental power and  $E_{nl}$  is the single pass conversion efficiency of the PPKTP crystal, which is given by the B-K expression [8]:

$$E_{nl} = \frac{4\omega^2 d_{\text{eff}}^2 L_C}{\varepsilon_0 c^3 \lambda_1 n_1 n_2} h(\alpha, \xi, \sigma) \exp[-(\alpha_1 + \alpha_2/2)L_C], \quad (2)$$

$$h(\alpha, \xi, \sigma) = \frac{1}{4\xi} \int_{-2\xi}^0 \int_{-2\xi}^0 dt dt' \frac{\exp[-\alpha(t+t'+2\xi) - i\sigma(t-t')]}{(1+it)(1-it')}, \quad (3)$$

where  $\omega$  is the angle frequency of FW,  $L_C$  represents the length of the PPKTP crystal,  $\varepsilon_0$  is the vacuum permittivity,  $c$  is the velocity of light in a vacuum and  $n_1$  and  $n_2$  are the refractive index of the FW and the HW in the crystal, respectively. The B-K focusing factor  $h$  depends on  $\alpha = (\alpha_1 - \alpha_2/2) \times z_R$ , the focusing parameter  $\xi = L_C/z_R$ , and the phase matching  $\sigma = \Delta k \times z_R$ , where  $\alpha_n$  ( $n = 1, 2$ ) is the absorption coefficient of the FW ( $n = 1$ ) and HW ( $n = 2$ ),  $z_R = \pi\omega_0^2 n_1 / \lambda_1$  is the Rayleigh range of the cavity mode, and  $\Delta k$  is the wave vector mismatching.

The circulating fundamental power  $P_C$  is specified by [39]:

$$P_C = \frac{P_1 \times T}{\left[1 - \sqrt{(1-T)(1-L)^2(1-\Gamma \times P_C)^2}\right]^2}, \quad (4)$$

where  $P_1$  is the fundamental power incident on the cavity,  $T$  is the transmission of the input coupler mirror,  $L$  is round-trip loss of the FW (excluding  $T$ ), respectively. The nonlinear loss  $\Gamma$  consists of  $E_{nl}$  and the efficiency of the HW absorption process  $\Gamma_{\text{abs}} = E_{nl} \times [\exp(\alpha \times L_C/2) - 1]$ , the SHG cavity conversion efficiency  $\eta = P_2/P_1$ . Using these known parameters of our SHG cavity ( $n_1 = 1.8302$ ,  $n_2 = 1.8894$  [40],  $\alpha_1 = 0.3\% \text{ cm}^{-1}$ ,  $\alpha_2 = 4.5\% \text{ cm}^{-1}$  [41],

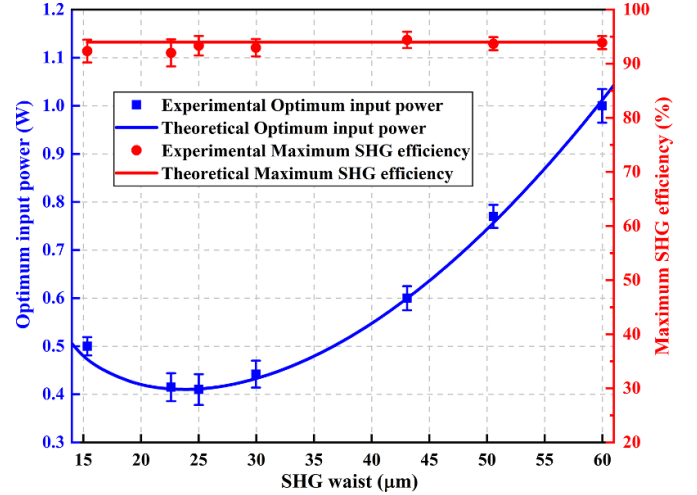


**Figure 2.** Input power as a function of the cavity waist at the optimal conversion efficiency. Red circles and red solid line are the experimental and fitted maximum conversion efficiency, respectively. Blue squares and blue solid line are the experimental and fitted input power, respectively.

and  $\varepsilon_0 = 8.85 \times 10^{-12} \text{ F m}^{-1}$ ), we fit the measurement results about the corresponding relationship between the beam waist  $\omega_0$  and input power at the optimal conversion efficiency, we obtained the unknown cavity parameters, including  $d_{\text{eff}}$ ,  $L$ , and  $T$ . The fitting results provide accurate parameters to infer the conversion efficiency from the pump depletion.

### 4. Experimental results and analysis

The conversion efficiencies are measured as a function of the input power at seven waist values  $\omega_0$ , from 15 to 60  $\mu\text{m}$ . For each waist value, the data points of the conversion efficiency versus the input power are excellently fitted to achieve a high conversion efficiency. The corresponding incident power versus the waist of the SHG cavity at the optimal conversion efficiency is shown in figure 2. As observed from the graph, the maximum frequency doubling efficiencies (>92%) are approximately the same under different cavity waists, demonstrating that it is not necessary to set the optimal cavity waist as mentioned in some literatures [24]. Due to the high circulating power benefited from the cavity enhancement, large nonlinear efficiency dominates the round trip loss, the conversion efficiency is insensitive to the focusing parameter [28, 42]. Additionally, looser focusing can help to mitigate the thermal effect, which becomes popular gradually [43, 44]. At the optimal conversion efficiency, the optimal incident power increases with a decrease in the waist in the cavity at  $\omega_0 < 25 \mu\text{m}$ . This occurs because a large angle of divergence in the cavity shortens the effective interaction length of the FW with the PPKTP crystal. At  $\omega_0 > 25 \mu\text{m}$ , the optimal input power gradually increases with  $\omega_0$ . Because the circuiting power density decreases with the looser focusing, higher power is required to compensate the reduction of the circulating power density.

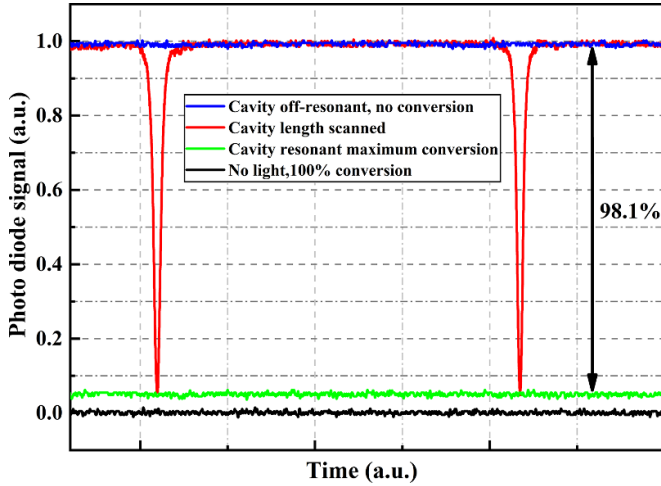


**Figure 3.** Depletion measurement for a fundamental input power of 1 W. Blue solid line and black line are SHG cavity off-resonant refers to 0% conversion and no light on PD2 reflection refers to 100% conversion, respectively. Green line represents SHG cavity of stabilized on maximum conversion. Red curve is scan of the cavity length of the TEM<sub>00</sub> mode. The maximum pump depletion is  $98.1 \pm 0.1\%$ .

We subsequently measure a pump depletion using PD2, which is shown in figure 3. According to the results described in figure 2, we choose the input power (1 W) and beam waist ( $60 \mu\text{m}$ ) to optimize the nonlinear conversion. The pump depletion is close to the mode-matching efficiency between the input beam and the SHG cavity at the optimal impedance-matching. When the fundamental mode resonates with the cavity, the other higher-order modes are off-resonance and cannot be coupled into the cavity. The reference for 0% conversion efficiency is the absence of FW light off the resonance cavity. When all light in front of the PD2 is blocked, a 100% conversion efficiency reference is measured. The red curve is detected when scanning the SHG cavity. The peak corresponds to the cavity resonance with the FW. The pump depletion from figure 3 is  $98.1 \pm 0.1\%$ . However, due to the non-perfect coating of the crystal, absorption that cannot be neglected occurs at this wavelength; therefore, the depleted pump power is not completely converted into the HW.

To accurately infer the conversion efficiency from the pump depletion, the ratio of the nonlinear depletion to the linear depletion must be quantified. When the sum of the nonlinear and linear depletion equals to the  $T$  value, the frequency-doubling cavity is impedance matched, corresponding to the working point with the highest conversion efficiency. Thus, the conversion efficiency can be deduced from the pump depletion once  $L$  and  $T$  are known. The conversion efficiency  $\eta$  is given by:

$$\eta = \eta_{\text{pd}} \times \frac{T - L}{T}. \quad (5)$$

According these known parameters and expression in section 3, we obtain the fitting results of the external cavity parameter ( $d_{\text{eff}}$ ,  $L$  and  $T$ ) by fitting the relationship between the beam waist  $\omega_0$  and the input power at the

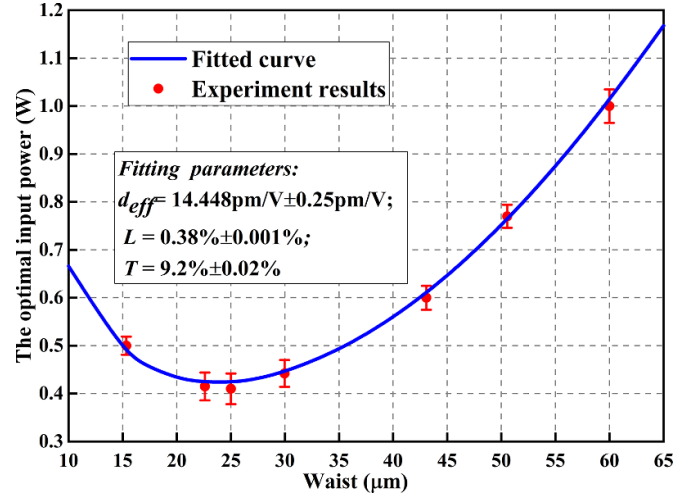


**Figure 4.** FW power versus cavity waist at the optimal conversion efficiency. Red circles and blue solid line are the experimental and fitted results, respectively.

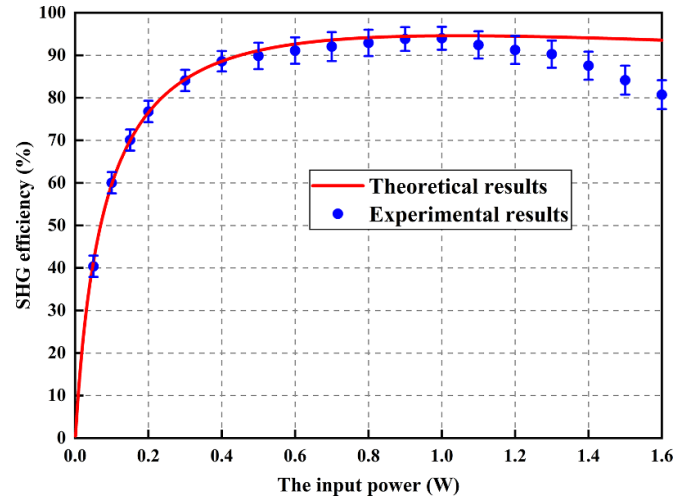


**Figure 5.** Theoretical and experimental SHG conversion efficiency versus incident power when the cavity waist is  $60 \mu\text{m}$ . Red solid line and blue circles are the theoretical and experimental results, respectively.

optimal conversion efficiency, which is shown in figure 4. We repeat the prior step ten times. The actual cavity parameters are shown below:  $d_{\text{eff}} = 14.448 \text{ pm V}^{-1} \pm 0.25 \text{ pm V}^{-1}$ ,  $L = 0.38 \pm 0.001\%$ ,  $T = 9.2 \pm 0.02\%$ . The maximum conversion efficiency is inferred to  $94.04 \pm 0.115\%$ . The results emphasize that the ultimate conversion efficiency of the external SHG process is determined by three factors:  $\eta_{\text{pd}}$ ,  $L$  and  $T$ , which provide a clear guideline to increase the conversion efficiency. The use of a high  $\eta_{\text{pd}}$  and low  $L$  is more popular. The higher  $T$  involves the challenge of increasing the input power as well; the  $T$  should be chosen according to the experimental condition. The maximum conversion efficiency is independent of the coefficient  $d_{\text{eff}}$ . However, a large  $d_{\text{eff}}$  can decrease the input power at the maximum conversion efficiency, which is helpful for the mitigation of the thermal effect.

The conversion efficiency of the SHG, as a function of the input power, is also measured using a commercial power meter (Thorlabs, S130C). The results are shown in figure 5 for a corresponding waist of 60  $\mu\text{m}$ . The temperature of the crystal is carefully optimized to obtain the maximum power of the HW for each data point. The experimental results in the low power region are in good agreement with the theoretical calculation. When the injected fundamental frequency optical power is 1 W, an HW output of 932 mW is obtained, with the original mode-matching of  $98.5 \pm 0.1\%$ ; the corresponding SHG conversion efficiency  $\eta_{\text{pm}}$  is 93.2%. Due to the large uncertainty of the power meter (3% @ 532 nm, 7% @ 1064 nm), the measurement result has an uncertainty of more than 3%. When the input power is increased beyond this point, the curves deviate from the theoretical results, which can be attributed to the weak thermal effect. Because the power meter introduces an uncertainty of more than 3%, the conversion efficiency  $\eta_{\text{pm}}$  has a larger uncertainty, compared with the  $\eta$  that is obtained using the pump depletion.

## 5. Conclusion

A pump depletion of 98.1% at a wavelength of 1064 nm is observed through the SHG process, in combination with the transmissivity  $T$  and the round-trip loss  $L$ , obtained from fitting the relationship between the  $\omega_0$  and input power at the optimal conversion efficiency; an inferred conversion efficiency of 94.04% is obtained with an uncertainty of 0.115%. In addition, a 93.2% conversion efficiency is obtained by the power meter measurement with an uncertainty of more than 3%. These results obtained from the two measurement methods are in good agreement, except for the uncertainty difference. The primary requirements for such a high-efficiency are the pump depletion  $\eta_{\text{pd}}$ , the low round-trip loss  $L$ , and the fitting transmissivity  $T$ . The maximum conversion efficiency is independent of the coefficient  $d_{\text{eff}}$ . However, the large  $d_{\text{eff}}$  can decrease the input power at the maximum conversion efficiency, which is helpful to mitigate the thermal effect. The same conversion efficiency is obtained in the waist range, from 15 to 60  $\mu\text{m}$ . Therefore, it is not necessary to set the focusing parameter at the optimal single-pass conversion. Using these results, one can conveniently design a high-efficiency frequency doubling system for numerous applications.

## Acknowledgments

The authors declare that they have no conflict of interest. This research was supported by National Natural Science Foundation of China (NSFC) (11654002, 11874250, and 11804207); National Key R&D Program of China (2016YFA0301401); Program for Sanjin Scholar of Shanxi Province; Key R&D Program of Shanxi (201903D111001); Fund for Shanxi '1331 Project' Key Subjects Construction; Program for Outstanding Innovative Teams of Higher Learning Institutions of Shanxi. Natural Science Foundation of Shanxi Province, China (201801D221006).

## References

- [1] Vahlbruch H, Mehmet M, Danzmann K and Schnabel R 2016 Detection of 15 dB squeezed states of light and their application for the absolute calibration of photoelectric quantum efficiency *Phys. Rev. Lett.* **117** 110801
- [2] Shi S, Wang Y, Yang W, Zheng Y and Peng K 2018 Detection and perfect fitting of 13.2 dB squeezed vacuum states by considering green-light-induced infrared absorption *Opt. Lett.* **43** 5411–4
- [3] Campagnola P J and Loew L M 2003 Second-harmonic imaging microscopy for visualizing biomolecular arrays in cells, tissues and organisms *Nat. Biotechnol.* **21** 1356–60
- [4] Chen X, Nadiarynkh O, Plotnikov S and Campagnola P J 2012 Second harmonic generation microscopy for quantitative analysis of collagen fibrillar structure *Nat. Protoc.* **7** 654–69
- [5] Eismann U, Gerbier F, Canalias C, Zukauskas A, Tréneç G, Vigué J, Chevy F and Salomon C 2012 An all-solid-state laser source at 671 nm for cold-atom experiments with lithium *Appl. Phys. B* **106** 25–36
- [6] Fonta F R, Marcum A S, Ismail A M and O'Hara K M 2019 High-power, frequency-doubled Nd:GdVO<sub>4</sub> laser for use in lithium cold atom experiments *Opt. Express* **27** 33144–58
- [7] Kleinman D A 1962 Theory of second harmonic generation of light *Phys. Rev.* **128** 1761
- [8] Boyd G D and Kleinman D A 1968 Parametric interaction of focused Gaussian light beams *J. Appl. Phys.* **39** 3597–639
- [9] Parameswaran K R, Kurz J R, Roussev R V and Fejer M M 2002 Observation of 99% pump depletion in single-pass second-harmonic generation in a periodically poled lithium niobate waveguide *Opt. Lett.* **27** 43–45
- [10] Levy J S, Foster M A, Gaeta A L and Lipson M 2011 Harmonic generation in silicon nitride ring resonators *Opt. Express* **19** 11415–21
- [11] Zhou Y J, Feng L Q and Sun J Q 2012 Single-mode propagation and highly efficient second harmonic generation in periodically poled MgO-doped LiNbO<sub>3</sub> on insulator rib waveguide *Chin. Phys. Lett.* **29** 084210
- [12] Kobayashi T, Akamatsu D, Nishida Y, Tanabe T, Yasuda M, Hong F L and Hosaka K 2016 Second harmonic generation at 399 nm resonant on the <sup>1</sup>S<sub>0</sub>-<sup>1</sup>P<sub>1</sub> transition of ytterbium using a periodically poled LiNbO<sub>3</sub> waveguide *Opt. Express* **24** 12142–50
- [13] Wolf R, Breunig I, Zappe H and Buse K 2017 Cascaded second-order optical nonlinearities in on-chip micro rings *Opt. Express* **25** 29927–33
- [14] Polzik E S and Kimble H J 1991 Frequency doubling with KNbO<sub>3</sub> in an external cavity *Opt. Lett.* **16** 1400–2
- [15] Yang W H, Wang Y J, Zheng Y H and Lu H D 2015 Comparative study of the frequency-doubling performance on ring and linear cavity at short wavelength region *Opt. Express* **23** 19624–33
- [16] Cruz L S and Cruz F C 2007 External power-enhancement cavity versus intracavity frequency doubling of Ti:sapphire lasers using BIBO *Opt. Express* **15** 11913–21
- [17] Cha Y H, Ko K H, Lim G, Han J M, Park H M, Kim T S and Jeong D Y 2010 Generation of continuous-wave single-frequency 15 W 378 nm radiation by frequency doubling of a Ti:sapphire laser *Appl. Opt.* **49** 1666–70
- [18] Kwon M, Yang P, Huft P, Young C, Ebert M and Saffman M 2020 Generation of 14.0 W of single-frequency light at 770 nm by intracavity frequency doubling *Opt. Lett.* **45** 339–42
- [19] Schneider K, Schiller S, Mlynek J, Bode M and Freitag I 1996 1.1-W single-frequency 532-nm radiation by second-harmonic generation of a miniature Nd:YAG ring laser *Opt. Lett.* **21** 1999–2001

- [20] Tian J F, Yang C, Xue J, Zhang Y C, Li G and Zhang T C 2016 High-efficiency blue light generation at 426 nm in low pump regime *J. Opt.* **18** 055506
- [21] Chen H Z, Liu X P, Wang X Q, Wu Y P, Wang Y X, Yao X C, Chen Y A and Pan J W 2018 30 W, sub-kHz frequency-locked laser at 532 nm *Opt. Express* **26** 33756–63
- [22] Cui S Z, Zhang L, Jiang H W, Pan W W, Yang X Z, Qin G S and Feng Y 2019 High efficiency frequency doubling with a passive enhancement cavity *Laser Phys. Lett.* **16** 035105
- [23] Targat R L, Zondy J J and Lemonde P 2005 75%-Efficiency blue generation from an intracavity PPKTP frequency doubler *Opt. Commun.* **247** 471–81
- [24] Lundeman J H, Jensen O B, Andersen P E, Andersson-Engels S, Sumpf B, Erbert G and Petersen P M 2008 High power 404 nm source based on second harmonic generation in PPKTP of a tapered external feedback diode laser *Opt. Express* **16** 2486–93
- [25] Villa F, Chiummo A, Giacobino E and Bramati A 2007 High-efficiency blue-light generation with a ring cavity with periodically poled KTP *J. Opt. Soc. Am. B* **24** 576–80
- [26] Ricciardi I, Rosa M D, Rocco A, Ferraro P and Natale P D 2010 Cavity-enhanced generation of 6 W cw second-harmonic power at 532 nm in periodically-poled MgO:LiTaO<sub>3</sub> *Opt. Express* **18** 10985–94
- [27] Zondy J J, Camargo F A, Zanon T, Petrov V and Wetter N U 2010 Observation of strong cascaded Kerr-lens dynamics in an optimally-coupled cw intracavity frequency-doubled Nd:YLF ring laser *Opt. Express* **18** 4796–815
- [28] Meier T, Willke B and Danzmann K 2010 Continuous-wave single-frequency 532 nm laser source emitting 130 W into the fundamental transversal mode *Opt. Lett.* **35** 3742–4
- [29] Han Y S, Wen X, Bai J D, Yang B D, Wang Y H, He J and Wang J M 2014 Generation of 130 mW of 397.5 nm tunable laser via ring-cavity-enhanced frequency doubling *J. Opt. Soc. Am. B* **31** 1942–7
- [30] Li Y, Zhou Z Y, Ding D S and Shi B S 2014 Low-power-pumped high-efficiency frequency doubling at 397.5 nm in a ring cavity *Chin. Opt. Lett.* **12** 111901–4
- [31] Zuo X J, Yan Z H and Jia X J 2019 High-efficiency generation of a low-noise laser at 447nm *Appl. Phys. Express* **12** 032010
- [32] Wang Q W, Tian L, Yao W X, Wang Y J and Zheng Y H 2019 Realizing a high-efficiency 426 nm laser with PPKTP by reducing mode-mismatch caused by the thermal effect *Opt. Express* **27** 28534–43
- [33] Ast S, Nia R M, Schonbeck A, Lastzka N, Steinlechner J, Eberle T, Mehmet M, Steinlechner S and Schnabel R 2011 High-efficiency frequency doubling of continuous-wave laser light *Opt. Lett.* **36** 3467–9
- [34] Cui X Y et al 2018 High-power 671 nm laser by second-harmonic generation with 93% efficiency in an external ring cavity *Opt. Lett.* **43** 1666–9
- [35] Li Z, Ma W, Yang W, Wang Y and Zheng Y 2016 Reduction of zero baseline drift of the Pound-Drever-Hall error signal with a wedged electro-optical crystal for squeezed state generation *Opt. Lett.* **41** 3331–4
- [36] Drever R W P, Hall J L, Kowalski F V, Hough J, Ford G M, Munley A J and Ward H 1983 Laser phase and frequency stabilization using an optical resonator *Appl. Phys. B* **31** 97–105
- [37] Wu L A and Kimble H J 1985 Interference effects in second-harmonic generation within an optical cavity *J. Opt. Soc. Am. B* **2** 697–703
- [38] Zhang H Y, Wang J R, Li Q H, Ji Y J, He Z Y, Yang R C and Tian L 2019 Experimental realization of high quality factor resonance detector *Acta Sin. Quantum Opt.* **25** 456
- [39] Kozlovsky W J, Nabors C D and Byer R L 1988 Efficient second harmonic generation of a diode-laser-pumped CW Nd:YAG laser using monolithic MgO:LiNbO<sub>3</sub> external resonant cavities *IEEE J. Quantum Electron.* **24** 913–9
- [40] Mehmet M 2012 Squeezed light at 1064 nm and 1550 nm with a nonclassical noise suppression beyond 10 dB PhD Thesis Leibniz Universität Hannover
- [41] Samanta G K, Kumar S C, Mathew M, Canalias C, Pasiskevicius V, Laurell F and Ebrahim-Zadeh M 2008 High-power, continuous-wave, second-harmonic generation at 532 nm in periodically poled KTiOPO<sub>4</sub> *Opt. Lett.* **33** 2955–7
- [42] Liu J L, Wang Z Y, Li H, Liu Q and Zhang K S 2011 Stable, 12 W, continuous-wave single-frequency Nd:YVO<sub>4</sub> green laser polarized and dual-end pumped at 880 nm *Opt. Express* **19** 6777–82
- [43] Paschotta R, Kürz P, Henking R, Schiller S and Mlynek J 1994 82% Efficient continuous-wave frequency doubling of 1.06 μm with a monolithic MgO:LiNbO<sub>3</sub> resonator *Opt. Lett.* **19** 1325–7
- [44] Wen X, Han Y S, Bai J D, He J, Wang Y H, Yang B D and Wang J M 2014 Cavity-enhanced frequency doubling from 795nm to 397.5nm ultra-violet coherent radiation with PPKTP crystals in the low pump power regime *Opt. Express* **22** 32293–300